

## Efficient Conversion of Syngas into Ethanol by Tandem Catalysis

Songyue Han, Dong Fan, Nan Chen, Wenhao Cui, Linhai He, Peng Tian,\* and Zhongmin Liu\*

Cite This: *ACS Catal.* 2023, 13, 10651–10660

Read Online

ACCESS |

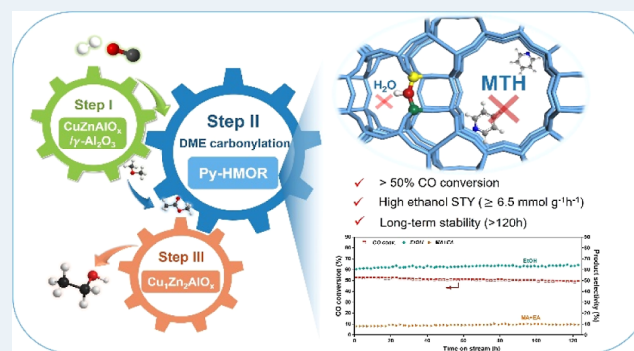
Metrics &amp; More

Article Recommendations

Supporting Information

**ABSTRACT:** Syngas conversion into ethanol by tandem catalysis has exhibited its potential for the selective production of ethanol. For practical applications, it is desired to develop a robust catalyst system to enhance the CO conversion while maintaining high selectivity to ethanol. Here, we report an efficient and stable triple-tandem catalyst system consisting of  $\text{CuZnAlO}_x/\gamma\text{-Al}_2\text{O}_3$ , pyridine-modified H-MOR zeolite (Py-HMOR), and  $\text{Cu}_1\text{Zn}_2\text{AlO}_x$ , which catalyzes syngas to dimethyl ether (DME), DME carbonylation to methyl acetate (MA), and MA hydrogenation to ethanol in tandem. Both high CO conversion (52%) and satisfying selectivity to ethanol (62%, excluding  $\text{CO}_2$ ) were achieved simultaneously, leading to an unprecedentedly high ethanol space-time yield of  $6.5 \text{ mmol g}^{-1} \text{ h}^{-1}$ . In situ DRIFT and control catalytic tests were designed to elucidate the intrinsic reason of the high activity and stability of Py-HMOR in the tandem system. The developed tandem catalyst system presents a promising prospect for the direct ethanol manufacture from syngas.

**KEYWORDS:** syngas, ethanol, carbonylation, MOR zeolite, tandem catalysis



## 1. INTRODUCTION

Syngas conversion into  $\text{C}_{2+}$  oxygenates has been arousing special interest in the catalysis field as it provides a promising production route for fuels and chemicals from non-petroleum resources such as coal, natural gas, and biomass.<sup>1,2</sup> Ethanol, as one of the most important  $\text{C}_{2+}$  oxygenates, has been widely employed for medical and energy purposes.<sup>3</sup> Conventionally, ethanol is manufactured via grain fermentation, which inevitably competes for food supplies of human beings.<sup>4,5</sup> Intensive efforts have been devoted to the direct synthesis of ethanol from syngas by using a single catalyst, including Rh-based, Mo-based, bi/multi-component catalysts, modified Fischer–Tropsch catalysts and modified methanol synthesis catalyst.<sup>6–15</sup> Pitifully, the catalytic efficacy of the reported catalysts is limited for practical applications (Table S1). The main obstacle lies in achieving satisfied ethanol selectivity, which demands an accurate control of C–C coupling between intermediate CO dissociative and non-dissociative activation species.<sup>16,17</sup> Mostly, the concurrence of multiple elementary reactions inevitably leads to the co-existence of multiple reaction channels and thus the broadened product spectrum.<sup>4,16</sup> Designing a system that could direct the reaction proceeding toward a single targeted reaction channel is the key for the high-selective preparation of ethanol from syngas.

Tandem/relay catalysis, in which different reactions are sequentially placed in cascade, provides an alternative route to control the reaction sequence and intermediates (Table S2).<sup>18–25</sup> Recently, Wang et al. designed a triple tandem catalytic system for syngas conversion, sequentially combining

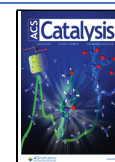
$\text{K}^+$ -modified  $\text{ZnO–ZrO}_2$ , H-MOR zeolite, and Pt–Sn/SiC catalysts, to achieve an ethanol selectivity of 90%.<sup>19</sup> This pioneering work preliminarily proved the efficacy of tandem catalysis for ethanol synthesis, involving the sequential occurrence of methanol synthesis, methanol carbonylation to acetic acid (AA), and hydrogenation of AA. The CO conversion was deliberately kept low, as the employed carbonylation catalyst requires higher CO partial pressure. The corresponding ethanol yield was thus far from satisfaction. Moreover, the presence of AA in the products can bring corrosive problem for the equipment, unfavorable for the practical applications. In another work by the same group, the AA intermediate was avoided by combining syngas to DME (STD), DME carbonylation to methyl acetate (MA), and MA hydrogenation in tandem.<sup>25</sup> As the optimum carbonylation catalyst only showed good stability at higher temperature (603–643 K), low CO conversion (<12%) was also observed due to thermodynamic limitations on the STD catalyst.

Developing an efficient carbonylation catalyst with high activity (even at higher CO conversion) and stability is thus the key for the tandem system. MOR zeolite, an important member of the zeolite family, is hitherto the most effective

Received: April 6, 2023

Revised: July 18, 2023

Published: July 31, 2023



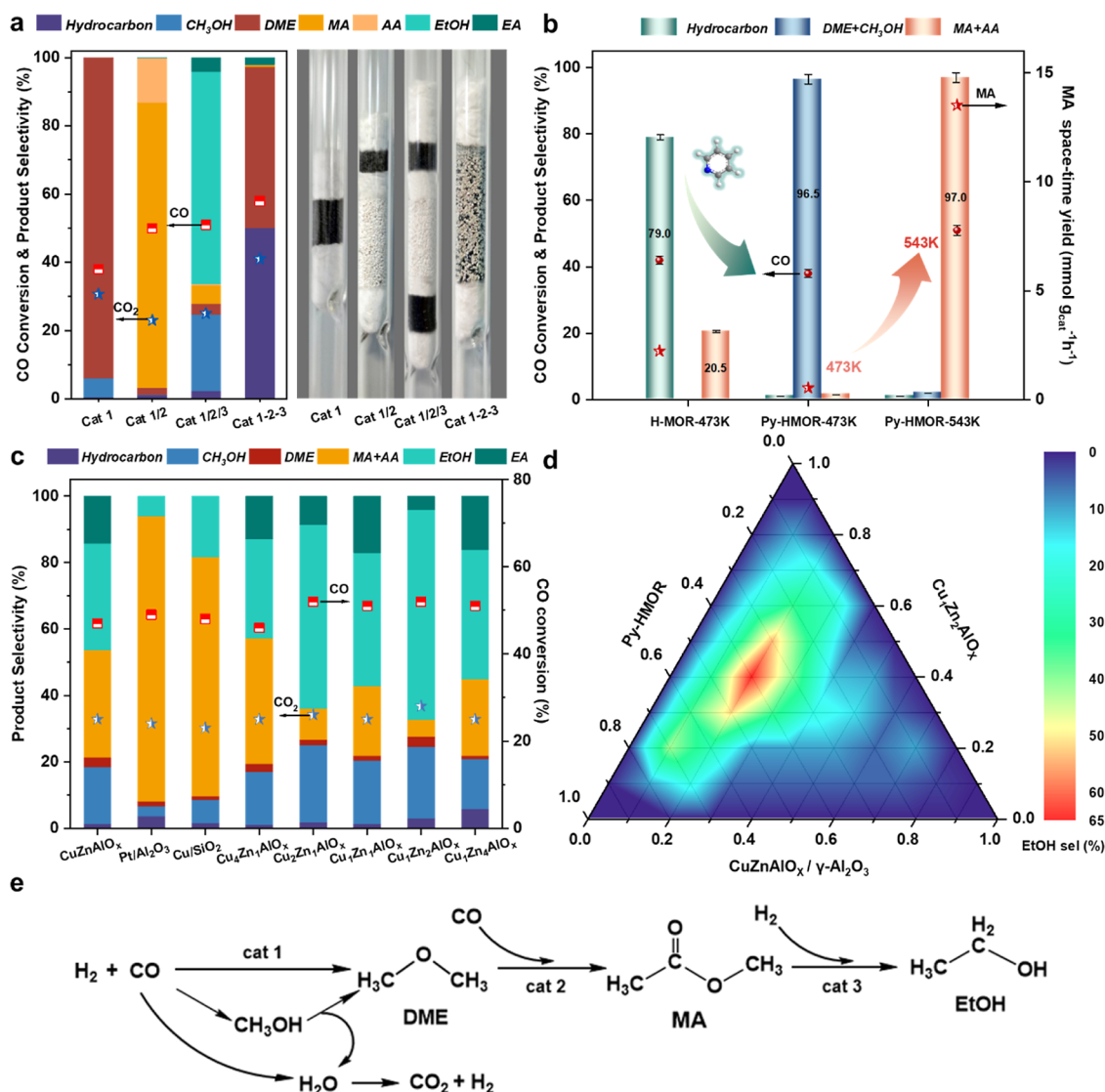


**Figure 1.** Catalyst performance of different combinations and ratio optimization. (a) Combinations and performance of the catalysts, cat 1: CuZnAlO<sub>x</sub>/γ-Al<sub>2</sub>O<sub>3</sub>; cat 2: Py-HMOR; and cat 3: Cu<sub>1</sub>Zn<sub>2</sub>AlO<sub>x</sub>. (b) Performance of Py-HMOR at 473 and 543 K in a dual-bed reactor. (c) Combinations of cat 1, cat 2, and hydrogenation catalysts. (d) Effect of catalyst mass ratio on ethanol selectivity. (e) Tandem reaction pathways for ethanol synthesis from syngas. Reaction conditions: H<sub>2</sub>/CO = 2, T = 543 K, P = 2.0 MPa, and F = 35 mL min<sup>-1</sup> (F = 70 mL min<sup>-1</sup> for cat 1); catalyst loading for (a), cat 1: 0.20 g; cat 1/2: 0.10 g/0.20 g; cat 1/2/3 (1-2-3): 0.10 g/0.20 g/0.20 g; for (b), the same as cat 1/2 in (a); for (c), the same as cat 1/2/3 in (a); for (d), the total weight of the catalysts is 0.50 g, and the coordinate scale represents the ratio of catalyst mass to total mass. MA: methyl acetate; AA: acetic acid; and EA: ethyl acetate. The selectivity of organics was calculated on a molar carbon basis (CO<sub>2</sub> free).

catalyst for DME carbonylation.<sup>26–29</sup> The Bronsted acid sites (BASs) in the 8-membered ring (8-MR) side pockets of MOR zeolite have been demonstrated to be the authentic catalytic centers, while those in 12-MR channels are prone to side reactions causing quick catalyst deactivation.<sup>30,31</sup> Several strategies have been reported to eliminate the acid sites in 12-MR channels and improve the catalytic performance, including SiCl<sub>4</sub> treatment,<sup>32</sup> amine modification,<sup>26,33,34</sup> and acid dealumination.<sup>35</sup> Besides, short diffusion length and low surface barrier<sup>36–39</sup> were also revealed to be positive for MOR zeolite to achieve better carbonylation performance.

In this paper, we report a robust triple-tandem catalyst system for syngas to ethanol, which involves the cooperation of CuZnAlO<sub>x</sub>/γ-Al<sub>2</sub>O<sub>3</sub> (for STD), pyridine-modified H-MOR (Py-HMOR, for DME carbonylation), and Cu<sub>1</sub>Zn<sub>2</sub>AlO<sub>x</sub> (for MA hydrogenation). Note that H-MOR nanocrystallites were synthesized and utilized as the precursor for the preparation of

high-efficiency carbonylation catalyst Py-MOR. The intermediate products and reaction atmosphere were precisely controlled to make the three reactions proceed in harmony, yielding high ethanol selectivity (62%), and ethanol yield (6.5 mmol g<sup>-1</sup> h<sup>-1</sup>). The crucial factors determining the catalytic activity and stability of the tandem system were investigated.

## 2. RESULTS AND DISCUSSION

### 2.1. Catalytic Performance of the Tandem System.

The tandem catalysis system for syngas conversion into ethanol herein involves the cooperation of three reactions, i.e., STD, DME carbonylation to MA, and the further hydrogenation of MA to ethanol. The three reactions are independent in nature, however, when placed in cascade, the factors influencing the catalytic performance of the reactions are interwoven, with the most notable influential factor of intermediate gas compositions. In order to realize high-

efficiency synthesis of ethanol, the incorporation of efficient catalyst for each reaction is certainly necessary. Meanwhile, the fine-tuning of the reaction conditions in a way that all three reactions proceed in a concerted way is equally important.

Different catalyst combinations and reaction conditions were consequently designed and tested, and the representative results are displayed in Figure 1. Note that the CO conversion of the first STD section is always kept low in the previous works in order to produce a relatively CO-enriched atmosphere in favor of the DME carbonylation section. However, the lower CO conversion undoubtedly hinders the improvement of the overall efficiency of the system. This dilemma promotes us to first investigate the optimal catalyst system and conditions for the STD with higher CO conversion. CuZnAlO<sub>x</sub> and  $\gamma$ -Al<sub>2</sub>O<sub>3</sub> composite catalysts with different ratios and proximity were prepared to catalyze the STD reaction (Figure S1), which indeed involved the sequential occurrence of CH<sub>3</sub>OH synthesis and its dehydration to DME. Among the various catalysts and reaction conditions (Table S3 and Figure S2), the powder-mixed CuZnAlO<sub>x</sub>/ $\gamma$ -Al<sub>2</sub>O<sub>3</sub> with a mass ratio of 2/1 showed the best catalytic performance with a CO conversion of 56% and a DME selectivity of 94% (excluding CO<sub>2</sub>) under conditions of 543 K, 2 MPa, and 10,000 mL g<sub>cat</sub><sup>-1</sup> h<sup>-1</sup>. The selectivity of CO<sub>2</sub> in the effluent product is about 31%, which implies the concurrence of the water-gas shift reaction (WGS, CO + H<sub>2</sub>O = CO<sub>2</sub> + H<sub>2</sub>) on CuZnAlO<sub>x</sub>. The consumption of H<sub>2</sub>O via the WGS reaction could lead to the right shift of the combined chemical equation (2CO + 4H<sub>2</sub> = DME + H<sub>2</sub>O), resulting in improved CO conversion. This is consistent with the results of thermodynamic equilibrium calculations that STD has a higher CO conversion than STM (Figure S3). In contrast, the catalytic performance of the quartz wool separated CuZnAlO<sub>x</sub>/ $\gamma$ -Al<sub>2</sub>O<sub>3</sub> catalyst is quite different, with a much lower CO conversion (12%) together with inferior DME selectivity, and no CO<sub>2</sub> could be detected in the product. This suggests the absence of the WGS reaction, as the H<sub>2</sub>O molecules produced by  $\gamma$ -Al<sub>2</sub>O<sub>3</sub> dehydration have no access to the CuZnAlO<sub>x</sub>. Powder-mixed CuZnAlO<sub>x</sub>/H-ZSM-5 is also tested for the STD section, which showed high initial CO conversion and DME selectivity (Figure S4). However, the reaction stability is inferior to CuZnAlO<sub>x</sub>/ $\gamma$ -Al<sub>2</sub>O<sub>3</sub>, possibly due to the fact that the methanol intermediate is more likely to undergo deeper reactions on the strong acid sites of H-ZSM-5. To summarize, powder-mixed CuZnAlO<sub>x</sub>/ $\gamma$ -Al<sub>2</sub>O<sub>3</sub> (mass ratio of 2/1) exhibits superior catalytic performance for the STD reaction, in terms of both catalytic activity and stability, and is consequently selected as the catalyst for the first stage of the tandem system.

A variety of zeolites were integrated as the second stage catalysts to catalyze the carbonylation of DME to produce MA (Table S4). The results show that the product selectivity was strongly dependent on zeolite topology (Figures S5–S8). Among the zeolites tested, a relatively high MA + AA selectivity of ca. 20% is observed on H-MOR. However, the co-production of large amounts of hydrocarbons implies the concurrence of methanol/DME to hydrocarbons (MTH) side reactions in the 12MR channels of MOR zeolite, which would undermine the long-term lifetime of the catalyst. To improve the MA selectivity and catalyst lifetime, metal-modified MOR was prepared and tested (Figure S9). Unfortunately, only limited amelioration could be observed.

Pyridine-modified H-MOR was further explored as the second-stage catalyst. Pyridine has been demonstrated to be

effective for selectively poisoning the acid sites in the 12-MR channels of MOR and inhibiting the MTH side reactions.<sup>26,36</sup> Given that DME carbonylation is commonly carried out in the temperature zone of 453–493 K on Py-HMOR,<sup>40–42</sup> a dual bed reactor was first chosen for the test, which allowed the sequential passage of syngas through CuZnAlO<sub>x</sub>/ $\gamma$ -Al<sub>2</sub>O<sub>3</sub> at 543 K and Py-HMOR held at a lower temperature (473 K). However, DME dominated the effluent products, while only a marginal amount of MA and AA could be detected (Figure 1b). To improve the carbonylation activity of Py-HMOR, its reaction temperature was elevated. From Figure S10, the MA + AA selectivity shows a gradual increase together with decreased DME proportion. No deactivation is observed during the 36 h test at 543 K. The CuZnAlO<sub>x</sub>/ $\gamma$ -Al<sub>2</sub>O<sub>3</sub> and Py-HMOR were further assembled into one reactor (separated by quartz wool), and similar to the results of the dual bed, a high CO conversion (50%) and MA + AA selectivity (97%, containing 12% of AA) were also realized at 543 K. It is noted that 543 K is rarely used for DME carbonylation on Py-HMOR, as quick deactivation commonly occurs at this high temperature. The unexpected stability of the tandem catalyst CuZnAlO<sub>x</sub>/ $\gamma$ -Al<sub>2</sub>O<sub>3</sub>|Py-HMOR will be further clarified in the Section 2.4.

To finalize the complete assembly of the triple tandem system, the hydrogenation catalyst was integrated after CuZnAlO<sub>x</sub>/ $\gamma$ -Al<sub>2</sub>O<sub>3</sub>|Py-HMOR to hydrogenate MA and obtain the target ethanol product (Figure 1c). Widely used Cu/SiO<sub>2</sub> and Pt/Al<sub>2</sub>O<sub>3</sub> catalysts only gave ethanol selectivity of 15 and 6.5%, respectively, implying their weak hydrogenation ability under the tested conditions. CuZnAlO<sub>x</sub> was also tested as the third-stage catalyst. In the resultant CuZnAlO<sub>x</sub>/ $\gamma$ -Al<sub>2</sub>O<sub>3</sub>|Py-HMOR|CuZnAlO<sub>x</sub> tandem system, an enhanced ethanol selectivity of 30% was observed. Optimization endeavors were subsequently carried out to enhance its hydrogenation capacity, mainly by adjusting the Cu/Zn ratios of the Cu<sub>a</sub>Zn<sub>b</sub>AlO<sub>x</sub> catalysts (Figures 1c, S11, and S12). For Cu<sub>4</sub>Zn<sub>1</sub>AlO<sub>x</sub> with the highest Cu content, a significant decay of ethanol selectivity was observed as the reaction proceeded, accompanied by an increased proportion of unreacted MA. Following the increase of ZnO content, both the catalytic stability and activity were significantly improved. The highest ethanol selectivity reached 62% over Cu<sub>1</sub>Zn<sub>2</sub>AlO<sub>x</sub> (Cu/Zn = 1:2 in mole), approaching the theoretical upper limit for ethanol selectivity (67% on a CO<sub>2</sub>-free base) via DME carbonylation. In the meantime, an overall CO conversion of 52% can be realized. This led to a significantly improved ethanol space-time yield (STY) of around 6.5 mmol g<sup>-1</sup> h<sup>-1</sup>, which should stand for the best value ever reported for syngas to ethanol (Table S2). In addition, small amounts of ethyl acetate (EA) were observed in the products, which should be formed by the esterification reaction between AA and ethanol over the acid sites of Cu<sub>1</sub>Zn<sub>2</sub>AlO<sub>x</sub> (Figure S13). The AA selectivity is below 0.1%, which implies negligible corrosion problem for the subsequent pipelines and equipment after the reactor.

The influence of catalyst mass ratios is illustrated in Figure 1d and Table S5. The zone colored in red represents the catalyst compositions with the best ethanol selectivity (55–63%), where the catalyst masses of the three stages are around 0.10, 0.20, and 0.20 g (1:2:2). Deviation from this ratio leads to a decreased ethanol selectivity. A higher loading of CuZnAlO<sub>x</sub>/ $\gamma$ -Al<sub>2</sub>O<sub>3</sub> in the first stage can result in a higher CO conversion and consequently a decreased CO partial pressure in the outlet of the first stage. This gas composition is

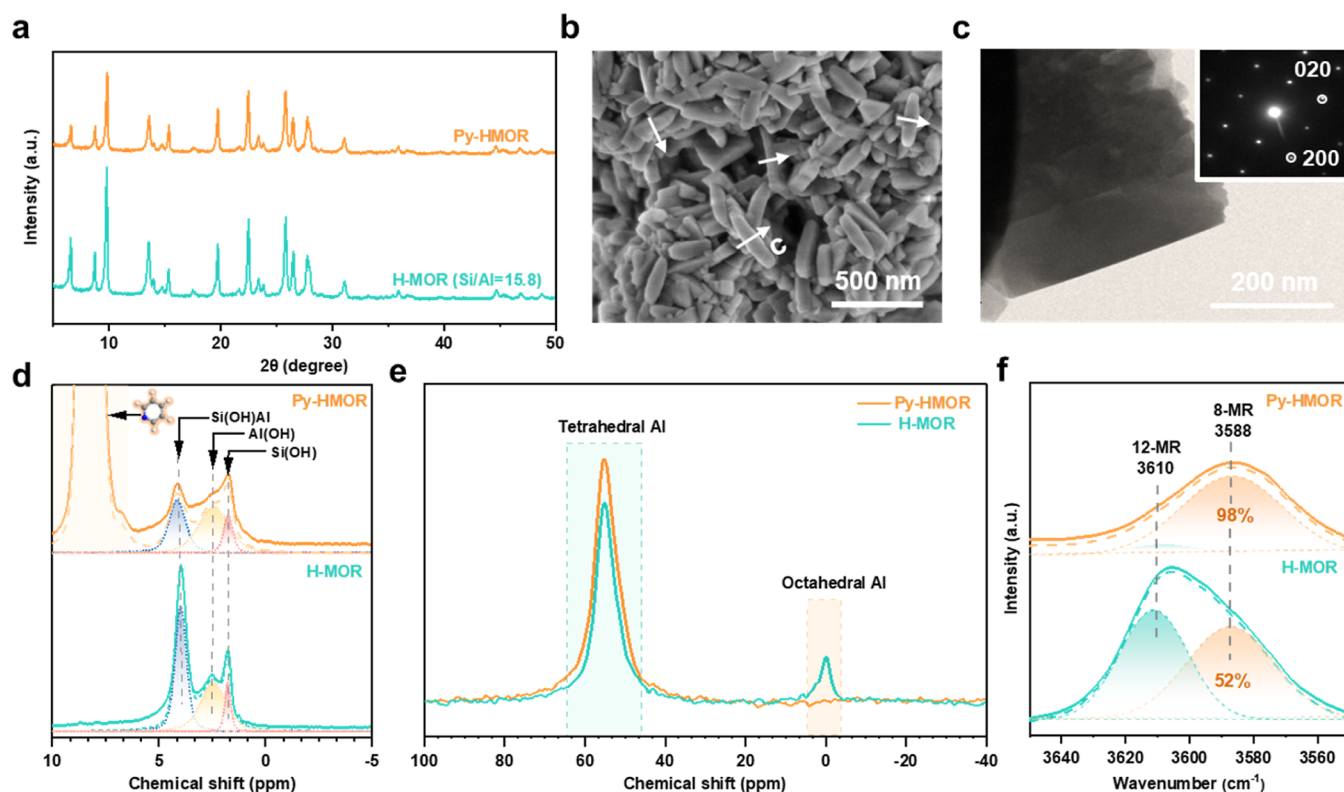


**Figure 2.** Characterization of MOR catalysts. (a) XRD patterns, (b) SEM image, (c) TEM image and SAED pattern, (d)  $^1\text{H}$  MAS NMR spectra, (e)  $^{27}\text{Al}$  MAS NMR spectra, and (f) acidic hydroxyl region of FT-IR spectra of the fresh catalysts. The arrows in (b) show the direction of  $c$ -axis. The numbers in (f) refer to the percentage of BASs in 8-MR.

not in favor of the catalytic efficiency of the second stage, as DME carbonylation activity is known to be in positive correlation with the partial pressure of CO. Moreover, the excessive loading of Py-HMOR would lead to a deficiency of DME in the atmosphere and decrease the catalyst stability. For the hydrogenation catalyst in the third stage, its overloading could further hydrogenate a considerable proportion of CO to methanol, leading to an increased methanol selectivity in the final product.

The effect of the catalyst proximity in the triple stages was further investigated by catalytic evaluation of the randomly mixed catalyst particles (Figure 1a). The products are dominated by aliphatic hydrocarbons including  $\text{CH}_4$ ,  $\text{C}_2$ – $\text{C}_4$  alkanes and olefins. The distinct catalytic behavior demonstrates that the sequential loading of the catalysts in the tandem system is pivotal for the targeted synthesis of ethanol, which ensures that the oxygenate intermediates follow the designed reaction pathway (Figure 1e).

**2.2. Catalyst Characterization.** Figure 2 displays the structural and acidity information of H-MOR and Py-HMOR. The XRD patterns evidence their high crystallinity with typical MOR structure (Figure 2a). SEM image indicates that the MOR zeolite has a nano slab morphology with diameter of 300 nm and thickness of 80 nm (Figure 2b). TEM image and selected area electron diffraction (SAED) pattern reveal that the short dimension of the crystals runs along the  $c$ -axis (Figure 2c), which would facilitate the mass transfer in the carbonylation reaction. The surface area and micropore volume of H-MOR determined by  $\text{N}_2$  physisorption are  $435 \text{ m}^2 \text{ g}^{-1}$  and  $0.14 \text{ cm}^3 \text{ g}^{-1}$ , respectively, confirming the good crystallinity of the sample. The  $^{27}\text{Al}$  MAS NMR spectra reveal that H-MOR contains tetrahedral Al species (55 ppm) and

small amounts of octahedral Al species (0 ppm).<sup>43</sup> However, the 0 ppm resonance is absent on Py-HMOR, implying that the octahedral Al in H-MOR is in effect framework-associated species and could be reconverted into tetrahedral coordination with the assistance of pyridine (Figure 2e).<sup>34</sup> The  $^1\text{H}$  MAS NMR spectra indicate that the Si(OH)Al signal at 3.9 ppm was significantly weakened after pyridine modification, while the signals of Si(OH) and Al(OH) were less affected (Figure 2d).<sup>44</sup> The density of BASs in the Py-HMOR is determined to be about 0.32 mmol/g. The BASs distribution is investigated by FT-IR. According to the deconvolution calculations, the percentage of BASs in 8-MR rises from 52% for H-MOR to 98% for Py-HMOR (Figure 2f). Moreover, similar weight loss curves (Figure S14) can be observed for Py-HMOR before and after 50 h of reaction, suggesting the negligible coke decomposition during the reaction. These results demonstrate that the BASs in the 12-MR of Py-HMOR are effectively covered by pyridine, consistent with the high selectivity and stability of Py-HMOR discussed in the above section.

The characterization results of hydrogenation catalysts  $\text{Cu}_x\text{Zn}_y\text{AlO}_x$  with different Cu/Zn ratios are presented in Figure S11. Following the increase of the Cu/Zn ratio, the XRD peaks ascribing to CuO are gradually augmented. The reduced catalysts  $\text{Cu}_1\text{Zn}_2\text{AlO}_x$  and  $\text{Cu}_4\text{Zn}_1\text{AlO}_x$  were further observed by XRD and TEM. The latter sample shows obviously strong XRD peaks arising from Cu species. From the TEM images, the average particle size of  $\text{Cu}_1\text{Zn}_2\text{AlO}_x$  is about 9.6 nm and the Cu species are uniformly dispersed in the ZnO phase. However, for  $\text{Cu}_4\text{Zn}_1\text{AlO}_x$  with higher Cu content, the average particle size increases to 40 nm. The results of  $\text{H}_2$ -TPR indicate that following the gradual increase of Cu/Zn ratio, the reduction peak becomes wide and moves toward high

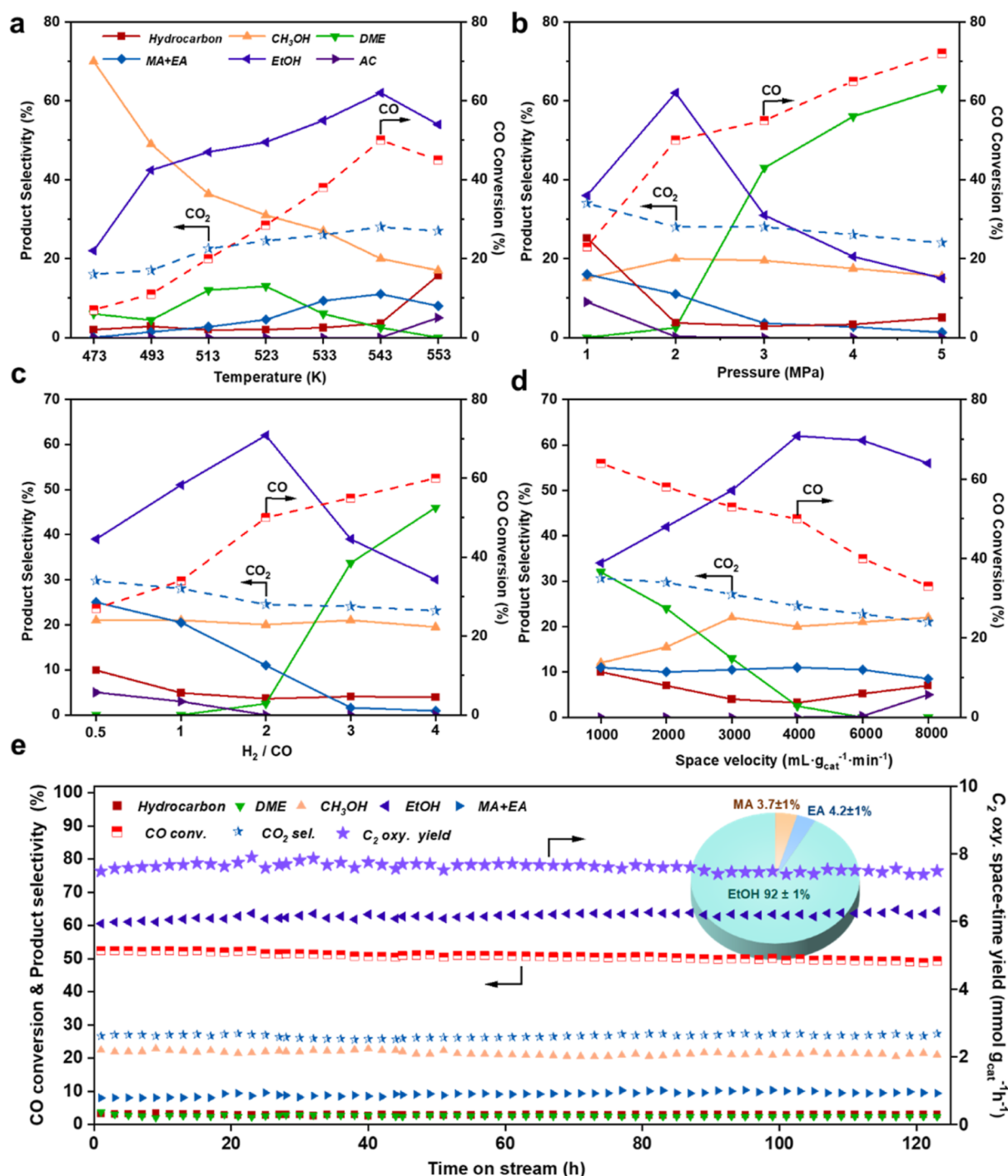


**Figure 3.** Catalytic performance of tandem system under different reaction conditions (a–d) and stability evaluation (e). The pie chart in (e) shows the distribution of C<sub>2</sub> oxygenates in the product. Reaction conditions for (a): H<sub>2</sub>/CO = 2, P = 2.0 MPa, and F = 35 mL min<sup>-1</sup>; for (b), H<sub>2</sub>/CO = 2, T = 543 K, and F = 35 mL min<sup>-1</sup>; for (c), T = 543 K, P = 2.0 MPa, and F = 35 mL min<sup>-1</sup>; for (d), H<sub>2</sub>/CO = 2; P = 2.0 MPa; and T = 543 K; for (e), H<sub>2</sub>/CO = 2, P = 2.0 MPa, T = 543 K, and F = 35 mL min<sup>-1</sup>; and weight of CuZnAlO<sub>x</sub>/γ-Al<sub>2</sub>O<sub>3</sub>, Py-HMOR, and Cu<sub>1</sub>Zn<sub>2</sub>AlO<sub>x</sub>: 0.10, 0.20, and 0.20 g. MA: methyl acetate; EA: ethyl acetate; AC: acetone; and C<sub>2</sub> oxy.: EtOH, MA, and EA. The selectivity of organics was calculated on a molar carbon basis (CO<sub>2</sub> free).

temperature. This implies an increased difficulty in reduction, arising from the large CuO particle sizes and their broadened distribution, which is in line with the XRD and TEM results. These results demonstrate that suitable Cu/Zn ratio is important for Cu<sub>a</sub>Zn<sub>b</sub>AlO<sub>x</sub> to maintain high Cu dispersion and thus to achieve high catalyst stability and MA hydrogenation activity.

**2.3. Effect of Reaction Conditions and Stability of Tandem Catalysts.** Figure 3a displays the catalytic performance of the triple tandem system (CuZnAlO<sub>x</sub>/γ-Al<sub>2</sub>O<sub>3</sub>|Py-HMOR|Cu<sub>1</sub>Zn<sub>2</sub>AlO<sub>x</sub>) at different temperatures. Following the temperature increase from 473 to 543 K, both CO conversion and ethanol selectivity rise significantly, although the reactions in the three stages are exothermic and thermodynamically more favorable at lower temperatures (Figures S15 and S16).

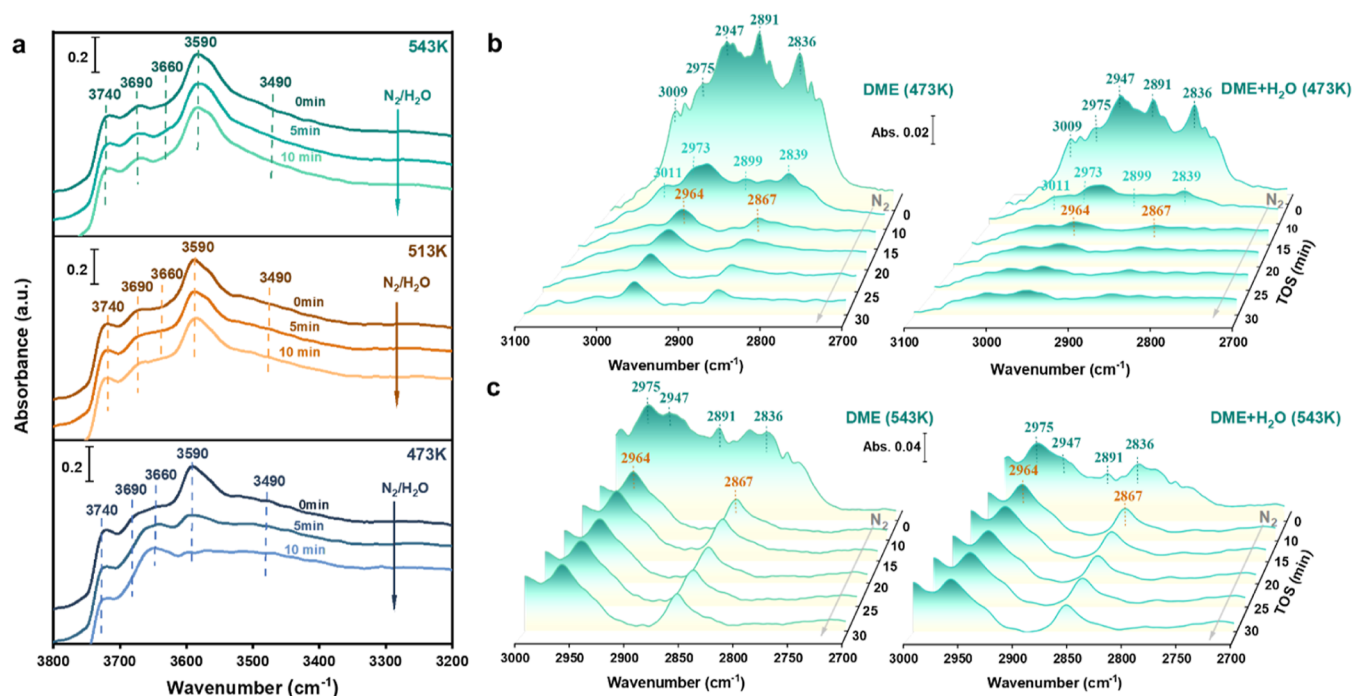


**Figure 4.** In situ DRIFT spectra of the effect of H<sub>2</sub>O on acidic hydroxyls and the formation of methoxy over Py-HMOR. (a) Dynamic changes of acidic hydroxyl groups after introducing H<sub>2</sub>O at different temperatures and normal pressure. (b,c) DME adsorption on Py-HMOR in the presence or absence of H<sub>2</sub>O at 473 K and 543 K. Adsorption conditions for (b,c):  $P = 2$  MPa, 5% DME in N<sub>2</sub> (35 mL min<sup>-1</sup>). For the introduction of H<sub>2</sub>O, 30 mL min<sup>-1</sup> of N<sub>2</sub> was passed through a water bath at 298 K at normal atmospheric pressure (a) or at 2 MPa (b,c).

Below 543 K, the overall tandem catalysis system is more likely to be kinetically controlled. At a lower temperature (e.g., 473 K), an obviously enriched CH<sub>3</sub>OH selectivity could be observed, possibly due to the weak dehydration ability of  $\gamma$ -Al<sub>2</sub>O<sub>3</sub> under this condition. With the further temperature rise to 553 K, the CO conversion declines, as thermodynamical limitations start to prevail over the kinetical limitations. Meanwhile, DME disappears in the products and hydrocarbon selectivity rises to 15%, showing the enhanced competition of side reactions (MA conversion) over Py-HMOR at high temperature. Besides, it is noted that about 5% of acetone (AC) is detected at 553 K, indicating the occurrence of new conversion pathway.

The reaction pressure also affects the catalytic behavior of the tandem system (Figure 3b). With the increase of pressure from 1 to 5 MPa, the CO conversion shows a monotonous increase from 23 to 73%, consistent with the thermodynamic analysis for the STD reaction (Figure S17). The ethanol selectivity increases in parallel with the pressure rising from 1 to 2 MPa, while an opposite trend is observed for MA + EA due to the enhanced hydrogenation capacity of Cu<sub>1</sub>Zn<sub>2</sub>AlO<sub>x</sub> at higher pressure. Moreover, the relatively high selectivity of hydrocarbons and acetone observed at 1 MPa implies the occurrence of side reactions on Py-HMOR, which should be caused by the higher CO partial pressure and complete DME conversion in the carbonylation section.<sup>41</sup> With the pressure increase from 2 to 5 MPa, the ethanol selectivity drops dramatically, accompanied by a notable increase of DME selectivity. This should be caused by the increased CO/DME ratio on Py-HMOR at 5 MPa, though the partial pressure of both CO and DME shows an increase. The existence of a large amount of unconverted DME cause the observed low ethanol selectivity.

Figure 3c shows the effect of H<sub>2</sub>/CO ratios on syngas conversion. Not surprisingly, the CO conversion rises with the increased H<sub>2</sub>/CO ratio, whereas an opposite trend is observed for selectivity of MA + AA. A similar volcano curve is observed for the variation trend of ethanol selectivity versus H<sub>2</sub>/CO ratios. The maximum ethanol selectivity is achieved with the H<sub>2</sub>/CO being 2. Further increasing the H<sub>2</sub>/CO ratio, the CO partial pressure becomes too low for DME carbonylation, leading to the low MA production in the second stage and consequently the decreased ethanol selectivity in the final product.

In addition, increasing the space velocity from 1000 to 8000 mL g<sup>-1</sup> h<sup>-1</sup> gave rise to a continuous decrease in CO conversion (Figure 3d). Below 4000 mL g<sup>-1</sup> h<sup>-1</sup>, the excessively high CO conversion is not favorable for MA formation, leading to the lower ethanol selectivity and larger amounts of DME residues. When the space velocity is higher than 4000 mL g<sup>-1</sup> h<sup>-1</sup>, the low CO conversion leads to an increased CO partial pressure and facilitates the carbonylation reaction over Py-HMOR. However, complete DME consumption caused increased selectivity of hydrocarbon and acetone. Moderate space velocity of 4000 mL g<sup>-1</sup> h<sup>-1</sup> should be a better choice, balancing CO conversion, ethanol selectivity, and catalyst stability.

The above results demonstrate that fine-tuning the reaction conditions in order that all the three reactions proceed in a concerted way is pivotal for the efficiency of the tandem system. According to the results, the optimal conditions for the triple tandem system is determined (543 K, 2 MPa, 4000 mL g<sup>-1</sup> h<sup>-1</sup> and H<sub>2</sub>/CO = 2). Based on this reaction condition, the long-term stability of the catalysts was tested (Figure 3e). The CO conversion was preserved above 50% during the 120 h lifetime test with no obvious deactivation. The ethanol selectivity is observed to be stably preserved above 60%

during the entire run. The total space-time yield of  $C_2$  oxygenates reached  $7.5 \text{ mmol g}^{-1} \text{ h}^{-1}$ , containing about 92 wt % of ethanol ( $6.5 \text{ mmol g}^{-1} \text{ h}^{-1}$ ) and 8 wt % of MA and EA. To the best of our knowledge, such a high ethanol synthesis efficiency has not ever been achieved for syngas conversion, be it via the direct or indirect approach (Table S2). Moreover, the spent catalysts after 120 h of reaction were characterized, and the results are displayed in Figure S18. No obvious change in crystal structure or particle sizes can be observed.

**2.4. Understanding the Activity and Stability of Py-HMOR in the Tandem System.** Various experiments were designed and carried out to understand the intrinsic reasons for the inferior catalytic activity of Py-HMOR at 473 K and its high stability at 543 K in the tandem system. It is speculated that the low activity at 473 K may be caused by the existence of a small amount of  $H_2O$  in the effluents from the first section. Moreover, the  $CH_3OH$  in the effluents can also exert negative influence as it yields  $H_2O$  when forming methoxy. This speculation was corroborated by the results of control experiments using simulated outlet compositions of the first-stage  $CuZnAlO_x/\gamma-Al_2O_3$  without  $H_2O$  or  $CH_3OH$  presence (Figure S19).

In situ DRIFTS experiments were further carried out to figure out the intrinsic reason on negative effect of  $H_2O$  molecules. It was revealed that  $H_2O$  molecules can interact with the acidic hydroxyls of zeolites, forming hydronium ions or hydrogen-bonding to acid sites.<sup>45</sup> The hydrolysis of Si–O–Al bonds would become inevitable under high  $H_2O$  partial pressure, which even causes the collapse of zeolitic framework.<sup>46</sup> Thus, the influence of  $H_2O$  on the acidic hydroxyls of Py-HMOR was first investigated by in situ DRIFTS. As illustrated in Figure 4a, the introduction of  $H_2O$  at 473 K leads to a rapid weakening of the peaks attributed to BASs ( $3590 \text{ cm}^{-1}$ ). Meanwhile, the peak at  $3660 \text{ cm}^{-1}$  presented a corresponding enhancement, which might arise from the hydronium ions.<sup>45</sup> With the increase of the temperature to 513 K, the influence of  $H_2O$  shows a significant attenuation. In addition, given that the presence of  $H_2O$  may affect the formation of methoxy from DME at the BASs,<sup>31</sup> Py-HMOR was pretreated with  $N_2/DME$  or  $N_2/DME/H_2O$  at 473 K and 2 MPa, followed by  $N_2$  purging and spectra collection to monitor the methoxy formation on the catalyst. From Figure 4b, before  $N_2$  purging, a multitude of absorption bands could be observed between  $2806$  and  $3009 \text{ cm}^{-1}$  due to the gas phase DME. Upon purging, these peaks disappear, and the hidden peaks at  $2964$  and  $2867 \text{ cm}^{-1}$  can be observed, which arise from surface methoxy formed by DME dissociation at the BASs.<sup>47</sup> However, cofeeding  $H_2O$  leads to an obviously reduced intensity of the bands, indicating that methoxy formation can be significantly perturbed by  $H_2O$  at 473 K. With the temperature elevated to 543 K,  $H_2O$  perturbation obviously abates, corroborated by the slightly weakened methoxy signals after cofeeding  $H_2O$  (Figures 4c and S20). Based on the above results, it can be summarized that at 473 K, the  $H_2O$  in the effluents from the first stage of tandem system competes with DME to interact with the acidic hydroxyls of Py-HMOR, disturbs the formation of methoxy, and causes the inferior activity of Py-HMOR. At 543 K, both the attenuated effect of  $H_2O$  and the accelerated reaction kinetics lead to the improved carbonylation activity of Py-HMOR.

Designed carbonylation reactions were carried out to understand the high catalytic stability of Py-HMOR at 543 K. From Figure S21, DME almost completely converted over

Py-HMOR at 573 K under simulated effluent from the first stage without  $H_2O$  or  $CH_3OH$  presence. The catalyst suffered fast deactivation after 10 h. In contrast, under similar conditions, a lower DME conversion and good catalyst stability are observed over the tandem system (Figure 3e). Evidently,  $H_2O$  perturbation toward DME carbonylation still exists at 543 K, although significantly attenuated compared with that at 473 K. These results suggest that the avoidance of complete DME conversion should be critical for catalyst stability, as DME deficiency can hinder the re-establishment of surface methoxy, undermine the catalytic cycles of carbonylation, and cause the occurrence of MA to hydrocarbons and subsequent catalyst deactivation. Additionally, the existence of  $H_2$  in the feed gas was also revealed to be positive for inhibiting coking and prolonging the catalyst stability (Figure S22). Figure 5 illustrates the crucial factors determining the carbonylation activity and stability of Py-HMOR in the tandem system.

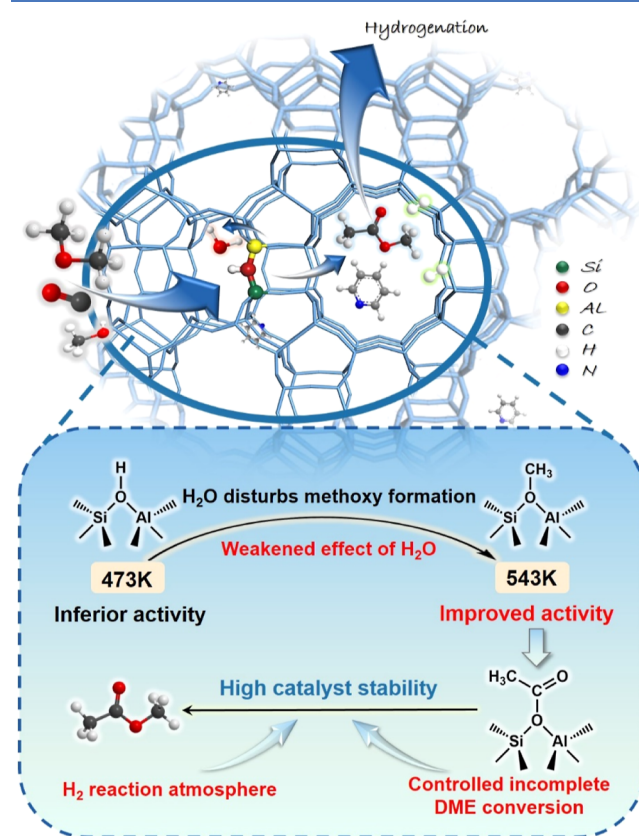


**Figure 5.** Illustration of the crucial factors determining the catalytic activity and stability of Py-HMOR in the tandem system.

### 3. CONCLUSIONS

A triple tandem catalyst system  $CuZnAlO_x/\gamma-Al_2O_3|Py-HMOR|Cu_1Zn_2AlO_x$  has been developed to efficiently convert syngas to ethanol. Under the optimized conditions, the CO conversion and ethanol selectivity can reach 52 and 62%, respectively, together with a high ethanol space-time yield of  $6.5 \text{ mmol g}^{-1} \text{ h}^{-1}$ .  $CuZnAlO_x/\gamma-Al_2O_3$  possesses higher catalytic stability than  $CuZnAlO_x/H-ZSM-5$  for the STD reaction. The unavoidable formation of small amounts of  $H_2O$  from the first stage can have a strong interaction with the acidic hydroxyls on Py-HMOR, disturb the methoxy formation, and

decrease the carbonylation activity, which however can be abated at an elevated temperature of 543 K. The excellent catalytic stability of Py-HMOR resulted from the contribution of pyridine modification, the controlled incomplete DME conversion (ensuring the formation of abundant methoxy and the smooth catalytic cycle), and the H<sub>2</sub> reaction atmosphere. This work demonstrates the promising application of tandem catalysis for the large-scale manufacturing of ethanol from syngas.

## ■ ASSOCIATED CONTENT

### SI Supporting Information

The Supporting Information is available free of charge at <https://pubs.acs.org/doi/10.1021/acscatal.3c01577>.

Experimental section; XRD patterns, TEM images, and H<sub>2</sub>-TPR profiles of CuZnAlO<sub>x</sub>/γ-Al<sub>2</sub>O<sub>3</sub> and Cu<sub>a</sub>Zn<sub>b</sub>AlO<sub>x</sub>; N<sub>2</sub> adsorption–desorption isotherms, NH<sub>3</sub>-TPD profiles, XRD patterns, and SEM images of different zeolites; catalytic performance of different types and treatment methods of molecular sieves combined with CuZnAlO<sub>x</sub>/γ-Al<sub>2</sub>O<sub>3</sub>; catalytic performance of Py-HMOR at different temperatures and with/without water and methanol in tandem system; Cu<sub>a</sub>Zn<sub>b</sub>AlO<sub>x</sub> catalytic stability tests and pyridine-adsorbed FT-IR spectrum of Cu<sub>1</sub>Zn<sub>2</sub>AlO<sub>x</sub>; TG curves of H-MOR and Py-HMOR after 50 h reaction and GC–MS chromatograms of organic materials retained in spent catalysts; thermodynamic calculation of synthesis gas to dimethyl ether/ethanol process; and FT-IR spectra of Py-HMOR at different temperatures (PDF)

## ■ AUTHOR INFORMATION

### Corresponding Authors

**Peng Tian** – National Engineering Research Center of Lower-Carbon Catalysis Technology, Dalian National Laboratory for Clean Energy, Dalian Institute of Chemical Physics, Chinese Academy of Sciences, Dalian 116023, China; [orcid.org/0000-0002-8768-0154](https://orcid.org/0000-0002-8768-0154); Email: [tianpeng@dicp.ac.cn](mailto:tianpeng@dicp.ac.cn)

**Zhongmin Liu** – National Engineering Research Center of Lower-Carbon Catalysis Technology, Dalian National Laboratory for Clean Energy, Dalian Institute of Chemical Physics, Chinese Academy of Sciences, Dalian 116023, China; [orcid.org/0000-0002-7999-2940](https://orcid.org/0000-0002-7999-2940); Email: [zml@dicp.ac.cn](mailto:zml@dicp.ac.cn)

### Authors

**Songyue Han** – National Engineering Research Center of Lower-Carbon Catalysis Technology, Dalian National Laboratory for Clean Energy, Dalian Institute of Chemical Physics, Chinese Academy of Sciences, Dalian 116023, China; University of Chinese Academy of Sciences, Chinese Academy of Sciences, Beijing 100049, China

**Dong Fan** – National Engineering Research Center of Lower-Carbon Catalysis Technology, Dalian National Laboratory for Clean Energy, Dalian Institute of Chemical Physics, Chinese Academy of Sciences, Dalian 116023, China

**Nan Chen** – National Engineering Research Center of Lower-Carbon Catalysis Technology, Dalian National Laboratory for Clean Energy, Dalian Institute of Chemical Physics, Chinese Academy of Sciences, Dalian 116023, China;

University of Chinese Academy of Sciences, Chinese Academy of Sciences, Beijing 100049, China

**Wenhao Cui** – National Engineering Research Center of Lower-Carbon Catalysis Technology, Dalian National Laboratory for Clean Energy, Dalian Institute of Chemical Physics, Chinese Academy of Sciences, Dalian 116023, China; University of Chinese Academy of Sciences, Chinese Academy of Sciences, Beijing 100049, China

**Linhai He** – National Engineering Research Center of Lower-Carbon Catalysis Technology, Dalian National Laboratory for Clean Energy, Dalian Institute of Chemical Physics, Chinese Academy of Sciences, Dalian 116023, China; University of Chinese Academy of Sciences, Chinese Academy of Sciences, Beijing 100049, China

Complete contact information is available at: <https://pubs.acs.org/doi/10.1021/acscatal.3c01577>

### Notes

The authors declare no competing financial interest.

## ■ ACKNOWLEDGMENTS

This work was supported by the National Natural Science Foundation of China (nos 22272173, 21991090, 21991091, and 22288101) and thanks to the funding from the Sino-French IRN (International Research Network).

## ■ REFERENCES

- (1) Liu, G. B.; Yang, G. H.; Peng, X. B.; Wu, J. H.; Tsubaki, N. Recent advances in the routes and catalysts for ethanol synthesis from syngas. *Chem. Soc. Rev.* **2022**, *51*, 5606–5659.
- (2) Zhou, W.; Cheng, K.; Kang, J. C.; Zhou, C.; Subramanian, V.; Zhang, Q. H.; Wang, Y. New horizon in C1 chemistry: breaking the selectivity limitation in transformation of syngas and hydrogenation of CO<sub>2</sub> into hydrocarbon chemicals and fuels. *Chem. Soc. Rev.* **2019**, *48*, 3193–3228.
- (3) Farrell, A. E.; Plevin, R. J.; Turner, B. T.; Jones, A. D.; O'Hare, M.; Kammen, D. M. Ethanol can contribute to energy and environmental goals. *Science* **2006**, *311*, 506–508.
- (4) Spivey, J. J.; Egbeki, A. Heterogeneous catalytic synthesis of ethanol from biomass-derived syngas. *Chem. Soc. Rev.* **2007**, *36*, 1514–1528.
- (5) Ragauskas, A. J.; Williams, C. K.; Davison, B. H.; Britovsek, G.; Cairney, J.; Eckert, C. A.; Frederick, W. J.; Hallett, J. P.; Leak, D. J.; Liotta, C. L.; et al. The path forward for biofuels and biomaterials. *Science* **2006**, *311*, 484–489.
- (6) Luan, X.; Ren, Z.; Dai, X.; Zhang, X.; Yong, J.; Yang, Y.; Zhao, H.; Cui, M.; Nie, F.; Huang, X. Selective Conversion of Syngas into Higher Alcohols via a Reaction-Coupling Strategy on Multifunctional Relay Catalysts. *ACS Catal.* **2020**, *10*, 2419–2430.
- (7) Morrill, M. R.; Thao, N. T.; Shou, H.; Davis, R. J.; Barton, D. G.; Ferrari, D.; Agrawal, P. K.; Jones, C. W. Origins of Unusual Alcohol Selectivities over Mixed Mg Al Oxide-Supported K/MoS<sub>2</sub> Catalysts for Higher Alcohol Synthesis from Syngas. *ACS Catal.* **2013**, *3*, 1665–1675.
- (8) Lin, T. J.; Qi, X. Z.; Wang, X. X.; Xia, L.; Wang, C. Q.; Yu, F.; Wang, H.; Li, S. G.; Zhong, L. S.; Sun, Y. H. Direct Production of Higher Oxygenates by Syngas Conversion over a Multifunctional Catalyst. *Angew. Chem., Int. Ed.* **2019**, *58*, 4627–4631.
- (9) Ma, C. H.; Li, H. Y.; Lin, G. D.; Zhang, H. B. Ni-decorated carbon nanotube-promoted Ni-Mo-K catalyst for highly efficient synthesis of higher alcohols from syngas. *Appl. Catal., B* **2010**, *100*, 245–253.
- (10) Wang, C. T.; Zhang, J.; Qin, G. Q.; Wang, L.; Zuidema, E.; Yang, Q.; Dang, S. S.; Yang, C. G.; Xiao, J. P.; Meng, X. J.; et al. Direct Conversion of Syngas to Ethanol within Zeolite Crystals. *Chem* **2020**, *6*, 646–657.

- (11) Sun, J.; Wan, S.; Wang, F.; Lin, J.; Wang, Y. Selective Synthesis of Methanol and Higher Alcohols over Cs/Cu/ZnO/Al<sub>2</sub>O<sub>3</sub> Catalysts. *Ind. Eng. Chem. Res.* **2015**, *54*, 7841–7851.
- (12) Haider, M. A.; Gogate, M. R.; Davis, R. J. Fe-promotion of supported Rh catalysts for direct conversion of syngas to ethanol. *J. Catal.* **2009**, *261*, 9–16.
- (13) Tien-Thao, N.; Hassanzahediniaki, M.; Alamdari, H.; Kaliaguine, S. Effect of alkali additives over nanocrystalline Co-Cu-based perovskites as catalysts for higher-alcohol synthesis. *J. Catal.* **2007**, *245*, 348–357.
- (14) Wang, Z.; Kumar, N.; Spivey, J. J. Preparation and characterization of lanthanum-promoted cobalt-copper catalysts for the conversion of syngas to higher oxygenates: Formation of cobalt carbide. *J. Catal.* **2016**, *339*, 1–8.
- (15) Zeng, Z.; Li, Z. S.; Guan, T.; Guo, S. X.; Hu, Z. W.; Wang, J. H.; Rykov, A.; Lv, J.; Huang, S. Y.; Wang, Y.; et al. CoFe alloy carbide catalysts for higher alcohols synthesis from syngas: Evolution of active sites and Na promoting effect. *J. Catal.* **2022**, *405*, 430–444.
- (16) Luk, H. T.; Mondelli, C.; Ferre, D. C.; Stewart, J. A.; Perez-Ramirez, J. Status and prospects in higher alcohols synthesis from syngas. *Chem. Soc. Rev.* **2017**, *46*, 1358–1426.
- (17) Ao, M.; Pham, G. H.; Sunarso, J.; Tade, M. O.; Liu, S. M. Active Centers of Catalysts for Higher Alcohol Synthesis from Syngas: A Review. *ACS Catal.* **2018**, *8*, 7025–7050.
- (18) Cao, Z.; Hu, T.; Guo, J.; Xie, J.; Zhang, N.; Zheng, J.; Che, L.; Chen, B. H. Stable and facile ethanol synthesis from syngas in one reactor by tandem combination CuZnAl-HZSM-5, modified-H-Mordenite with CuZnAl catalyst. *Fuel* **2019**, *254*, 115542.
- (19) Kang, J.; He, S.; Zhou, W.; Shen, Z.; Li, Y.; Chen, M.; Zhang, Q.; Wang, Y. Single-pass transformation of syngas into ethanol with high selectivity by triple tandem catalysis. *Nat. Commun.* **2020**, *11*, 827.
- (20) Upham, D. C.; Orazov, M.; Jaramillo, T. F. Phosphate-passivated mordenite for tandem-catalytic conversion of syngas to ethanol or acetic acid. *J. Catal.* **2021**, *399*, 132–141.
- (21) Zhang, Y.; San, X. G.; Tsubaki, N.; Tan, Y. S.; Chen, J. F. Novel Ethanol Synthesis Method via C1 Chemicals without Any Agriculture Feedstocks. *Ind. Eng. Chem. Res.* **2010**, *49*, 5485–5488.
- (22) Zhang, Y. K.; Ding, C. M.; Wang, J. W.; Jia, Y. M.; Xue, Y. A.; Gao, Z. T.; Yu, B.; Gao, B. Z.; Zhang, K.; Liu, P. Intermediate product regulation over tandem catalysts for one-pass conversion of syngas to ethanol. *Catal. Sci. Technol.* **2019**, *9*, 1581–1594.
- (23) Wei, Q. H.; Yang, G. H.; Gao, X. H.; Tan, L.; Ai, P. P.; Zhang, P. P.; Lu, P.; Yoneyama, Y.; Tsubaki, N. A facile ethanol fuel synthesis from dimethyl ether and syngas over tandem combination of Cu-doped HZSM35 with Cu-Zn-Al catalyst. *Chem. Eng. J.* **2017**, *316*, 832–841.
- (24) Li, X.; San, X.; Zhang, Y.; Ichii, T.; Meng, M.; Tan, Y.; Tsubaki, N. Direct Synthesis of Ethanol from Dimethyl Ether and Syngas over Combined H-Mordenite and Cu/ZnO Catalysts. *ChemSusChem* **2010**, *3*, 1192–1199.
- (25) Zhou, W.; Kang, J.; Cheng, K.; He, S.; Shi, J.; Zhou, C.; Zhang, Q.; Chen, J.; Peng, L.; Chen, M.; et al. Direct Conversion of Syngas into Methyl Acetate, Ethanol, and Ethylene by Relay Catalysis via the Intermediate Dimethyl Ether. *Angew. Chem., Int. Ed.* **2018**, *57*, 12012–12016.
- (26) Liu, J. L.; Xue, H. F.; Huang, X. M.; Wu, P. H.; Huang, S. J.; Liu, S. B.; Shen, W. J. Stability Enhancement of H-Mordenite in Dimethyl Ether Carbonylation to Methyl Acetate by Pre-adsorption of Pyridine. *Chin. J. Catal.* **2010**, *31*, 729–738.
- (27) Cao, K. P.; Fan, D.; Zeng, S.; Fan, B. H.; Chen, N.; Gao, M. B.; Zhu, D. L.; Wang, L. Y.; Tian, P.; Liu, Z. M. Organic-free synthesis of MOR nanoassemblies with excellent DME carbonylation performance. *Chin. J. Catal.* **2021**, *42*, 1468–1477.
- (28) Liu, Y. H.; Zhao, N.; Xian, H.; Cheng, Q. P.; Tan, Y. S.; Tsubaki, N.; Li, X. G. Facilely Synthesized H-Mordenite Nanosheet Assembly for Carbonylation of Dimethyl Ether. *ACS Appl. Mater. Interfaces* **2015**, *7*, 8398–8403.
- (29) Chen, N.; Zhang, J.; Gu, Y. T.; Zhang, W. N.; Cao, K. P.; Cui, W. H.; Xu, S. T.; Fan, D.; Tian, P.; Liu, Z. M. Designed synthesis of MOR zeolites using gemini-type bis(methylpyrrolidinium) dications as structure directing agents and their DME carbonylation performance. *J. Mater. Chem. A* **2022**, *10*, 8334–8343.
- (30) Rasmussen, D. B.; Christensen, J. M.; Temel, B.; Studt, F.; Moses, P. G.; Rossmeisl, J.; Riisager, A.; Jensen, A. D. Reaction mechanism of dimethyl ether carbonylation to methyl acetate over mordenite a combined DFT/experimental study. *Catal. Sci. Technol.* **2017**, *7*, 1141–1152.
- (31) Boronat, M.; Martinez-Sanchez, C.; Law, D.; Corma, A. Enzyme-like Specificity in Zeolites: A Unique Site Position in Mordenite for Selective Carbonylation of Methanol and Dimethyl Ether with CO. *J. Am. Chem. Soc.* **2008**, *130*, 16316–16323.
- (32) Liu, R. S.; Fan, B. H.; Zhang, W. N.; Wang, L. Y.; Qi, L.; Wang, Y. L.; Xu, S. T.; Yu, Z. X.; Wei, Y. X.; Liu, Z. M. Increasing the Number of Aluminum Atoms in T-3 Sites of a Mordenite Zeolite by Low-Pressure SiCl<sub>4</sub> Treatment to Catalyze Dimethyl Ether Carbonylation. *Angew. Chem., Int. Ed.* **2022**, *61*, No. e202116990.
- (33) Liu, S. P.; Liu, H. C.; Ma, X. G.; Liu, Y.; Zhu, W. L.; Liu, Z. M. Identifying and controlling the acid site distributions in mordenite zeolite for dimethyl ether carbonylation reaction by means of selective ion-exchange. *Catal. Sci. Technol.* **2020**, *10*, 4663–4672.
- (34) Liu, R. S.; Fan, B. H.; Zhi, Y. C.; Liu, C.; Xu, S. T.; Yu, Z. X.; Liu, Z. M. Dynamic Evolution of Aluminum Coordination Environments in Mordenite Zeolite and Their Role in the Dimethyl Ether (DME) Carbonylation Reaction. *Angew. Chem., Int. Ed.* **2022**, *61*, No. e202210658.
- (35) Xue, H. F.; Huang, X. M.; Zhan, E. S.; Ma, M.; Shen, W. J. Selective dealumination of mordenite for enhancing its stability in dimethyl ether carbonylation. *Catal. Commun.* **2013**, *37*, 75–79.
- (36) Cao, K. P.; Fan, D.; Li, L. Y.; Fan, B. H.; Wang, L. Y.; Zhu, D. L.; Wang, Q. Y.; Tian, P.; Liu, Z. M. Insights into the Pyridine-Modified MOR Zeolite Catalysts for DME Carbonylation. *ACS Catal.* **2020**, *10*, 3372–3380.
- (37) Liu, Z. Q.; Yi, X. F.; Wang, G. R.; Tang, X. M.; Li, G. C.; Huang, L.; Zheng, A. M. Roles of 8-ring and 12-ring channels in mordenite for carbonylation reaction: From the perspective of molecular adsorption and diffusion. *J. Catal.* **2019**, *369*, 335–344.
- (38) Cao, K. P.; Fan, D.; Gao, M. B.; Fan, B. H.; Chen, N.; Wang, L. Y.; Tian, P.; Liu, Z. M. Recognizing the Important Role of Surface Barriers in MOR Zeolite Catalyzed DME Carbonylation Reaction. *ACS Catal.* **2022**, *12*, 1–7.
- (39) Liu, S. P.; Cheng, Z. Z.; Li, Y.; Sun, J. H.; Cai, K.; Huang, S. Y.; Lv, J.; Wang, S. P.; Ma, X. B. Improved Catalytic Performance in Dimethyl Ether Carbonylation over Hierarchical Mordenite by Enhancing Mass Transfer. *Ind. Eng. Chem. Res.* **2020**, *59*, 13861–13869.
- (40) Cheung, P.; Bhan, A.; Sunley, G. J.; Law, D. J.; Iglesia, E. Site requirements and elementary steps in dimethyl ether carbonylation catalyzed by acidic zeolites. *J. Catal.* **2007**, *245*, 110–123.
- (41) Cheung, P.; Bhan, A.; Sunley, G. J.; Iglesia, E. Selective carbonylation of dimethyl ether to methyl acetate catalyzed by acidic zeolites. *Angew. Chem., Int. Ed.* **2006**, *45*, 1617–1620.
- (42) Zhan, E. S.; Xiong, Z. P.; Shen, W. J. Dimethyl ether carbonylation over zeolites. *J. Energy Chem.* **2019**, *36*, 51–63.
- (43) Chen, K. Z.; Gan, Z. H.; Horstmeier, S.; White, J. L. Distribution of Aluminum Species in Zeolite Catalysts: <sup>27</sup>Al NMR of Framework, Partially-Coordinated Framework, and Non-Framework Moieties. *J. Am. Chem. Soc.* **2021**, *143*, 6669–6680.
- (44) Hayashi, S.; Kojima, N. Acid properties of H-type mordenite studied by solid-state NMR. *Microporous Mesoporous Mater.* **2011**, *141*, 49–55.
- (45) Siria, J. C.; Duran, M.; Lledós, A.; Bertrán, J. Acid-catalyzed hydrogenation of olefins. A theoretical study of the hydrogen fluoride and H<sub>3</sub>O<sup>+</sup> catalyzed hydrogenation of ethylene. *J. Am. Chem. Soc.* **1987**, *109*, 7623–7629.

(46) Smith, L.; Cheetham, A. K.; Morris, R. E.; Marchese, L.; Thomas, J. M.; Wright, P. A.; Chen, J. On the nature of water bound to a solid acid catalyst. *Science* **1996**, *271*, 799–802.

(47) Campbell, S. M.; Jiang, X. Z.; Howe, R. F. Methanol to hydrocarbons: spectroscopic studies and the significance of extra-framework aluminium. *Microporous Mesoporous Mater.* **1999**, *29*, 91–108.